BBA - Biomembranes 1864 (2022) 184005

Contents lists available at ScienceDirect

BBA - Biomembranes

journal homepage: www.elsevier.com/locate/bbamem

Vinca alkaloid binding to P-glycoprotein occurs in a processive manner

Shagufta Iqbal [a], Caitlin Flux [a], Deborah A. Briggs [b], Evelyne Deplazes [c], Jiansi Long [a], Ruth Skrzypek [a], Alice Rothnie [d], Ian D. Kerr [b], Richard Callaghan [a,e,*]

[a] Division of Biomedical Science & Biochemistry, Research School of Biology, The Australian National University, Canberra, Australia
[b] School of Life Sciences, University of Nottingham, Queen's Medical Centre, Nottingham, UK
[c] School of Chemistry and Molecular Biosciences, University of Queensland, St Lucia, Australia
[d] Health & Life Sciences, Aston University, Aston Triangle, Birmingham, UK
[e] School of Biomedical Sciences, Faculty of Biological Science, University of Leeds, Leeds, UK

ARTICLE INFO

Keywords:
P-glycoprotein
Multidrug resistance
Membrane transport
ABC protein
Drug binding
ABCB1

ABSTRACT

A mechanistic understanding of how P-glycoprotein (Pgp) is able to bind and transport its astonishing range of substrates remains elusive. Pharmacological data demonstrated the presence of at least four distinct binding sites, but their locations have not been fully elucidated. The combination of biochemical and structural data suggests that initial binding may occur in the central cavity or at the lipid-protein interface. Our objective was to define the binding sites for two transported substrates of Pgp; the anticancer drug vinblastine and the fluorescent probe rhodamine 123. A series of mutations was generated in positions proximal to previously defined drug-interacting residues on Pgp. The protein was purified and reconstituted into styrene-maleic acid lipid particles (SMALPs) to measure the apparent drug binding constant or into liposomes for assessment of drug-stimulated ATP hydrolysis. The biochemical data were reconciled with structural models of Pgp using molecular docking. The data indicated that the binding of rhodamine 123 occurred predominantly within the central cavity of Pgp. In contrast, the significantly more hydrophobic vinblastine bound to both the lipid-protein interface and within the central cavity. The data suggest that the initial interaction of vinca alkaloids with Pgp occurs at the lipid interface followed by internalisation into the central cavity, which also provides the transport conduit. This model is supported by recent structural observations with Pgp and early biophysical and cross-linking approaches. Moreover, the proposed model illustrates that the broad substrate profile for Pgp is underpinned by a combination of multiple initial interaction sites and an accommodating transport conduit.

1. Introduction

The ATP Binding Cassette (ABC) transporter P-glycoprotein (Pgp; ABCB1) is characterised by an astonishing range of substrates; a feature labelled as poly-specificity. Substrates share little consistent chemical, pharmacological or structural features and the pharmacophore of interaction is not completely understood. Attempts to define the pharmacophore have been restricted to physical features including hydrophobicity, planarity and the presence of a cationic nitrogen group [1,2].

P-gp expression in cancer cells is associated with a multidrug resistance phenotype and its impacts on patient survival, the incidence of remission and contribution to the failure of chemotherapy are compelling. Moreover, Pgp is expressed at numerous barrier or excretory sites in the body and it contributes significantly to shaping the pharmacokinetic profile of many drugs.

An understanding of the precise location of binding sites for drugs on Pgp will help to define the drug pharmacophore. Numerous research teams pursued this information using a broad range of distinct experimental approaches [3–8]. Site directed mutagenesis was the first strategy and identified a large number of potential drug-binding residues spread throughout the protein sequence [9,10]. Photoaffinity labelling with drug analogues and subsequent proteolytic cleavage revealed several regions of the protein involved in drug binding; almost exclusively within the transmembrane domains [5,8,11]. Improvements in our understanding of Pgp topography and the initial low-resolution, structural data posited that the binding sites were located within the central cavity and at the lipid-protein interface [3,12,13]. The presence of an annular drug binding region seemed appropriate given the hydrophobicity of many P-gp substrates and two elegant studies supported this [14,15].

* Corresponding author at: School of Biomedical Sciences, Faculty of Biological Science, University of Leeds, Leeds, UK.
E-mail address: r.callaghan@leeds.ac.uk (R. Callaghan).

https://doi.org/10.1016/j.bbamem.2022.184005
Received 29 November 2021; Received in revised form 8 July 2022; Accepted 12 July 2022
Available online 19 July 2022

During this period there were also a number of alternative suggestions to explain the polyspecificity of Pgp. The most prominent likened the protein to a hydrophobic *vacuum cleaner* and suggested that the binding interaction did not follow classic receptor pharmacology [15,16]. However, multiple investigations using steady-state transport, drug stimulated ATPase activity and radioligand binding measures reaffirmed the classic dogma [17–20]. Moreover, these approaches revealed that P-gp contained multiple specific binding sites that are connected by a complex allosteric interaction.

An elegant photo-crosslinking and mass spectrometry-based approach suggested that some hydrophobic drugs interact with Pgp via the lipid milieu at the juxtaposition of transmembrane helices TM3/8 and between TM5/11 [8]. These locations have been likened to gates that open into the central cavity of Pgp. The central cavity has been identified by comprehensive mutagenesis analyses to contain the sites for binding of rhodamine 123 (R-site) and Hoechst 33342 (H-site) [21–24]. More recently, we have compared the regions involved in the binding of four compounds with distinct chemical and physical features. This investigation [7] demonstrated the presence of multiple putative binding sites and suggested that they were located either within the central cavity, or at the protein-lipid interface.

The Pgp structure generated by Nosol et al. [25] using cryo-EM provided further support for the cavity/gate depiction of substrate binding. This investigation described P-gp structures (occluded with antibody fragments) with bound inhibitors to provide insight into binding. Inhibitors were suggested to bind in pairs, one in the central cavity and the other at a phenylalanine-rich access tunnel between the cavity and an annular binding site. This intriguing occluded configuration of Pgp may represent a transitional protein state subsequent to the unbound or basal conformation. It provides the first clue that inhibitors may transit between the annular and cavity sites.

In the present manuscript we have extended our earlier work to provide a more detailed map of drug binding to Pgp. Early investigations by our team established the presence of at least *four pharmacologically distinct binding sites for different drugs* on Pgp [19] and defining their locations remains crucial to understanding the enigmatic property of polyspecificity in pumps. Over a period of over two decades, mutagenesis-led investigations identified a large number of amino-acids potentially involved in substrate binding to Pgp (summarised in [26]). Structural data posits the *central cavity* of Pgp as the site for the interaction of more hydrophilic compounds [27] such as rhodamine 123, but this may simply be a *transport conduit*. Moreover, we have identified three putative sites [7] that are located on Pgp at the *lipid interface*. In the present manuscript, we have focussed primarily on the binding sites for rhodamine 123 (cavity) and vinblastine (interface). Using structural data described by the *4M1M*-model of Pgp [28], we have identified amino-acids proximal to contact residues for the binding of rhodamine 123 and vinblastine to mutate. Experimental parameters were reconciled, using computational methods, with a structural model of P-gp to assess the contributions of interface and cavity sites to substrate binding.

2. Materials & methods

2.1. Materials

Insect cells were cultured in Insect-Xpress (Lonza - Gordon, NSW) or Ex-Cell 405 (Merck - Castle Hill, NSW) supplemented with heat inactivated foetal bovine serum (Bovagen, East Keilor, Vic). For the extraction and purification of P-glycoprotein, n-Dodecyl-β-D-Maltopyranoside was obtained from Anatrace (Ohio, USA) and the total *E. coli* lipids from Avanti Polar Lipids (Alabama, USA). SMA powder was a kind gift from Cray Valley (Houston, USA). For chromatography, Ni-NTA His·Bind resin was purchased from Merck (Bayswater, Vic), gel permeation PD10 columns from VWR (Tingalpa, Qld) and BioBead SM-2 resin from Bio-Rad (Gladesville, NSW). Cholesterol, disodium adenosine triphosphate, nicardipine hydrochloride, vinblastine sulphate and rhodamine123 were purchased from Merck (Castle Hill, NSW). All general laboratory chemicals were obtained from standard laboratory suppliers and were of at least analytical grade.

2.2. Production of mutant P-gp and recombinant baculovirus

Mutations were introduced at 8 positions into a cysteine free, C-terminally His-tagged version of P-gp [29] encoded in a baculovirus expression system compatible plasmid (pFastBac_MCHS; [30]) as previously described [7]. Single cysteine isoforms F72C (TM1), F193C (TM3), F194C (TM3), A198C (TM3), S344C (TM6), Y950C (TM11), Y953C (TM11) and I981C (TM12) were generated and sub-cloned into pFastBac_MCHS. This enabled the generation of Bacmid DNA in *E. coli* DH10Bac competent cells as described [31]. Bacmid DNA was verified by PCR amplification and confirmed by sequencing bacmid PCR products. High titre recombinant baculoviruses were produced following transfection of Bacmid DNA into serum free Sf9 cells [31].

The choice of mutations is based on the mouse structure for Pgp (PDB 4M1M) and of the eight residues selected for mutation in human Pgp, seven of them are conserved with the mouse isoform. The human V981 position is similar to the equivalent residue in the mouse sequence (I977). The mouse Pgp isoforms (*mdr1-2*) have high sequence conservation with the human isoform, a finding replicated in functional analyses. Subtle differences from human Pgp in the cellular resistance to colchicine have been reported for mouse mdr1/mdr3 [32]. However, the affinity of binding to Pgp for vinca alkaloids and anthracyclines are similar between mouse and human Pgp [29,33].

2.3. Cell culture and membrane production

Trichoplusia ni (High-Five) cells (1–2 × 10^6) were infected with recombinant baculovirus at a multiplicity of infection of 2 to express each mutant version of Pgp. The cells were grown for a period of three days post-infection and subsequently harvested by centrifugation. Harvested cells were disrupted by nitrogen cavitation [29] and crude membranes were prepared using differential ultracentrifugation. Membranes were stored at −80 °C at a protein concentration of 30–50 mg ml^{-1}.

2.4. P-gp purification using SMA extraction

Insect cell membranes were re-suspended in solubilisation buffer (20 mM MOPS, 200 mM NaCl, pH 8.0) containing 0.75 % (w/v) styrene maleic acid (SMA) at a concentration of 30 mg ml^{-1} wet weight of the membrane (adapted from [34]). The mixture was spun at 41,200 g (20 min) after an incubation at room temperature for 2 h with constant stirring. The supernatant was mixed with Ni-NTA His·Bind resin at volumetric ratio of 1:15 and gently stirred overnight at 4 °C. The protein was purified with immobilised metal affinity chromatography following binding in a gravity-based system. The resin was washed to remove unbound and contaminating proteins with 5 column volumes (CV) of buffer (20 mM MOPS, 200 mM NaCl, pH 8.0) containing 10 mM or 20 mM imidazole. The protein was eluted from resin in 400 mM imidazole containing buffer. Following purification, PD10 gel permeation columns (GE Healthcare) were used to remove imidazole as per the manufacturer's instructions. The buffer exchanged protein was concentrated to 1 ml using Amicon ™ Ultracentrifugal filters with a 100 kDa cut-off filter. The concentrated protein was quantified using densitometric analysis (Image J) of quantitative SDS-PAGE with known amounts of BSA (bovine serum albumin) as standard.

2.5. P-gp purification using dodecyl-maltoside extraction

P-gp was purified from crude membranes (30-100 mg) suspended at 5 mg ml^{-1} protein using immobilised metal affinity chromatography (IMAC), according to previously published methods [7,31]. Solubilisation was achieved using 2 % (w v^{-1}) dodecyl-β-D-maltoside (DDM) in

buffer supplemented with a 0.4 % (w v^{-1}) lipid mixture (4:1 ratio of *E. coli* extract:cholesterol). The DDM solubilised P-gp was mixed by stirring for 120 min at 4 °C. Following binding to the Ni-NTA His·Bind Resin (1 ml per 100 mg starting membrane), protein was eluted with 400 mM imidazole. The chromatography buffers (pH 6.8) were supplemented with 0.1 % (w v^{-1}) DDM and 0.1 % (w v^{-1}) lipid mixture and reconstitution was achieved using detergent adsorption to SM-2 Bio-Beads [29].

2.6. Measurement of drug binding to Pgp – tryptophan quenching assay

Binding of drugs to purified Pgp encapsulated within SMALPs was measured through the quenching of the fluorescence of endogenous tryptophan residues [35] using the conditions previously described [7]. The SMALP system was used to measure tryptophan quenching since it offers considerably improved resolution of fluorescence spectra due to reduced scattering effects [36].

Tryptophan fluorescence from purified protein (50 μg) was measured in a total cuvette volume of 1 ml (200 mM NaCl, 20 mM MOPS pH 8.0). Fluorescence spectra of the intrinsic tryptophan residues were recorded at $\lambda_{excitation} = 295 \pm 5$ nm and an emission range from $\lambda = 300$–500 nm (emission slit width = 5 nm). All drugs (2–50 μM) were sequentially added from concentrated stocks in DMSO and the amount of solvent was maintained at ≤1 % (v v^{-1}) [18].

For drugs that altered the emission intensity at λ_{max}, the intensity was plotted as a function of drug concentration. A secondary hyperbolic relationship plot was fitted, by non-linear regression with the binding isotherm; $B = (FS_{MAX}[D])/(K_{App} + [D])$. The change in fluorescence intensity revealed the extent of drug binding, FS_{MAX} is the maximal change in fluorescence observed, K_{App} is the apparent binding affinity and [D] is the drug concentration.

2.7. Measurement of ATP hydrolysis by Pgp – colorimetric assay

ATP hydrolysis was determined by measurement of the rate of inorganic phosphate liberation by Pgp containing proteoliposomes (0.1–0.5 μg protein per point) using a modified colorimetric assay [7,37]. Analysis used:

(i) varying concentrations of ATP (0–2.5 mM) in the presence (i.e. stimulated activity) or absence (i.e. basal activity) of 10 μM nicardipine, or,
(ii) varying drug concentration (10^{-9} to 10^{-4} M) in the presence of fixed ATP (2 mM).

In both cases incubation was for 40 min, 37 °C prior to termination of the reaction and addition of colorimetric reagents. The absorbance at λ = 750 nm was measured for all samples using an iMark Microplate reader and the amount of phosphate liberated was determined from a standard curve of inorganic phosphate (0–20 nmol P_i).

The Michaelis-Menten parameters of ATP affinity (K_M) and maximal velocity (V_{MAX}) were derived from plots of activity (v) as a function of ATP concentration (S) using:

$$v = (V_{MAX} \times [S])/(K_M + [S]).$$

Drug ([D]) potency (EC_{50}) and the extent of ATPase activity stimulation (v) were estimated by non-linear regression of the general dose-response relationship:

$$v = v_{initial} + \left(v_{final} - v_{initial}\right)/\left(1 + 10^{(log10(EC_{50} - [D]))}\right),$$

where $v_{initial}$ is the activity in the absence of drug and v_{final} is the maximal activity observed.

The SMALP system was not used for ATPase assays since magnesium results in precipitation of styrene maleic acid [36].

2.8. Molecular drug docking to Pgp

The substrates vinblastine and rhodamine 123 were docked onto the structure of mouse P-glycoprotein [3] following a number of refinements (PDB file *4M1M*) [28]. The PDB files for the drugs and the protein chain A were converted to an AutoDock Vina compatible format (PDBQT) using MGL Tools (version 1.5.6) as previously described [38]. For the first set of drug docking, the entire transmembrane domain (TMD) was selected with the dimensions of 38 Å × 50 Å × 34 Å centred on the middle axis of the protein as the search space for AutoDock Vina. The second set of docking for vinblastine was restricted to the one-half of the TMD with the dimensions of 22 Å × 26 Å × 22 Å including the residues identified through experimental data. The docked binding modes were visualised and analysed using PyMOL (version 2.3.4) and VMD [39].

2.9. Statistical and quantitative analyses

Activity and binding data were quantitatively analysed with non-linear least square regression using GraphPad Prism 5. ANOVA was used to compare (Dunnett's post-hoc test) different mutant forms of P-glycoprotein and the differences with $P < 0.05$ were defined as significant.

3. Results

3.1. Preparation of purified Pgp

Cysless P-gp extracted from High-5 insect cell membranes with DDM was purified as shown in Fig. 1a. Analysis of SDS-PAGE using Image J indicated a purity of 85 ± 3 % and the yield of Pgp was 1.2 ± 0.2 μg mg^{-1} (membrane protein). Fig. 1b shows the extraction and purification of cysless Pgp using SMA. The final yield of Pgp was 0.68 ± 0.19 μg mg^{-1} (wet weight membrane) and with a purity of 81 ± 1 %.

3.2. Activity of purified Pgp reconstituted into liposomes

The ATPase activity of cysless Pgp is shown under basal conditions (drug free) and in the presence of 10 μM nicardipine (Fig. 2a). Under basal conditions, the affinity for ATP was $K_M = 1.1 \pm 0.2$ mM and a maximal velocity of $V_{MAX} = 455 \pm 68$ nmol min^{-1} mg^{-1} (n = 7). In the presence of nicardipine the affinity for ATP was similar ($K_M = 0.7 \pm 0.1$ mM), however the maximal velocity was increased to $V_{MAX} = 1763 \pm 304$ nmol min^{-1} mg^{-1}, which represents a 3.8 ± 0.5-fold stimulation.

Fig. 2b shows the maximal velocity obtained for the entire series of mutations in Pgp in the absence or presence of nicardipine (10 μM), which is known to stimulate ATPase activity. All mutant forms of Pgp used in this investigation displayed basal and drug stimulated ATPase activity that was broadly similar to the control cysless form. Both the basal and stimulated activities of mutants A198C and S344C were significantly higher ($P < 0.05$) than cysless Pgp; whilst the degree of stimulation remained unchanged. The effects of F72C, Y950C and I981C mutations on ATP hydrolysis did not reach statistical significance. The key observation is that all mutant forms of P-gp were functionally viable and thus enabled further characterisation of drug-protein interaction.

This investigation is focussed on binding sites for two transported substrates on Pgp, one of which is thought to be located within the central cavity and the site for rhodamine 123 interaction [7,22,40]. The second site is believed to interact with the significantly more hydrophobic compound vinblastine and is likely to be located at the protein-lipid interface [7,15]. To measure drug interaction with P-gp, the strategy employs two primary assays. The ATPase assay reveals the extent to which a drug may stimulate hydrolysis and the potency of this effect. The second measures the quenching of intrinsic tryptophan fluorescence in the presence of bound drug. Not all tryptophan residues are proximal to bound drug and the assay thereby provides a measure of

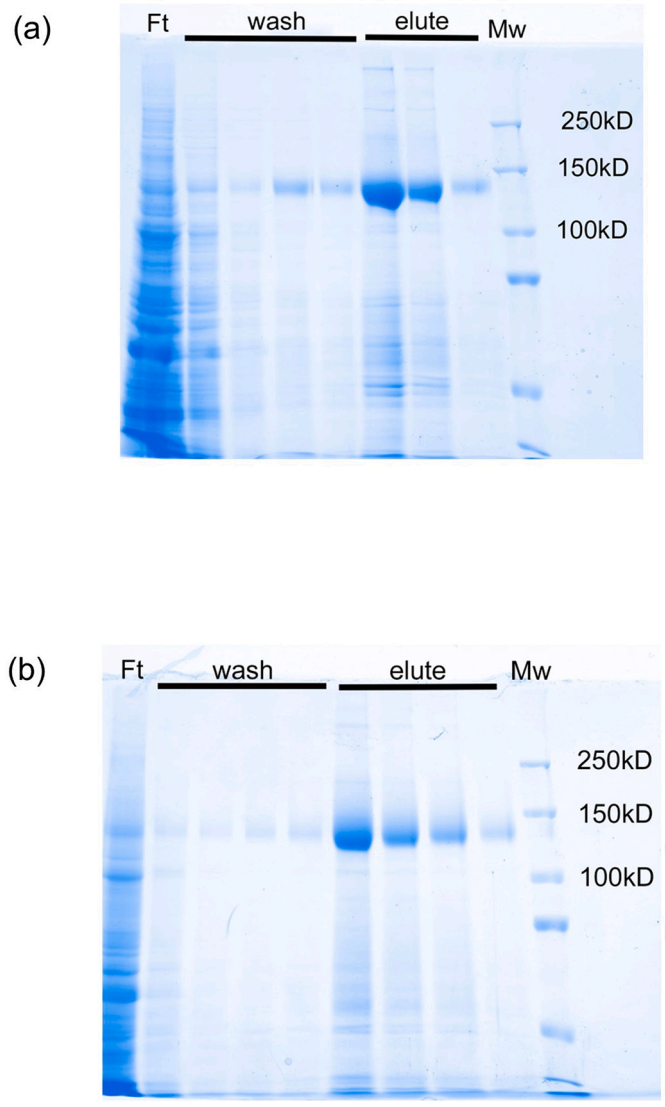

Fig. 1. Purification of Pgp following extraction by dodecyl-maltoside or styrene-maleic acid.
Analyses of cysless Pgp purified from High-5 cell membranes following extraction by (a) dodecyl-β-maltoside, or (b) styrene maleic acid. Aliquots (4 % of total volume) from the loading (Ft), wash and elution fractions were loaded onto 8 % SDS-PAGE gels and proteins detected with Instant Blue stain. The lane marked Mw contains pre-stained protein molecular weight markers.

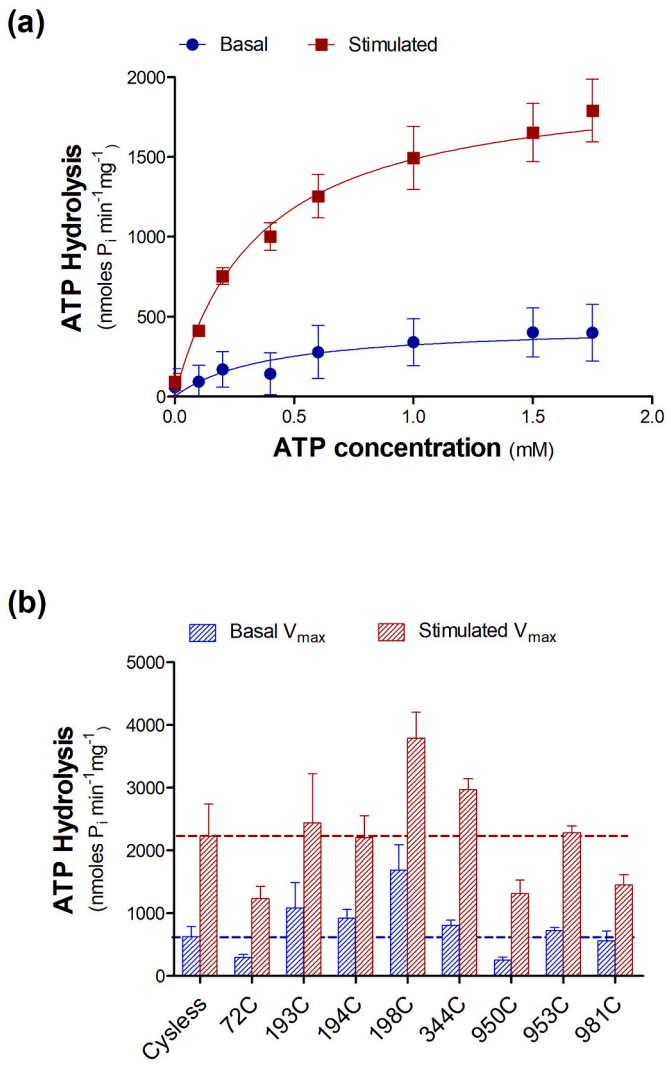

Fig. 2. Michaelis-Menten parameters for ATPase activity of Pgp.
The ATPase activity of purified Pgp reconstituted into liposomes was measured at a range of ATP concentrations in the presence or absence of nicardipine.
(a) Basal and nicardipine (10 μM) stimulated activities were plotted as a function of ATP concentration for cysless Pgp and fitted by the hyperbolic Michaelis-Menten equation. Values represent the mean ± SEM from n = 7 independent observations.
(b) The V_{MAX} obtained for basal and stimulated activity is shown for cysless and mutated P-gp. The blue and red dashed lines represent V_{MAX} for basal and stimulated activity respectively. Values represent the mean ± SEM from n = 3–8 independent observations.

apparent binding affinity and it has been widely used to characterise binding to Pgp [35,41]. Data from the two substrates was also compared to that of the inhibitor nicardipine which is known to interact at a pharmacologically distinct site to vinblastine and rhodamine 123, based on the presence of allosteric interactions [19]. Furthermore, our recent publication suggests that nicardipine interacts at an interfacial site, but one that is distinct from the proposed vinblastine site [7].

Fig. 3 illustrates the type of primary data obtained from the ATPase activity assay in the presence of either vinblastine or rhodamine 123, with Table 1 (and Figs. S1, S2) encompassing fitted data for all mutants with both substrates. Where stimulation occurs, the data was fitted using non-linear regression of the general dose-response relationship. The ATPase activity of cysless Pgp was stimulated 1.94 ± 0.09-fold by vinblastine (n = 8), with a potency of 2.69 ± 0.52 μM (Fig. 3a–b, Table 1). The data shown (Fig. 3a) for the F193C mutation highlights a situation wherein the extent of stimulation by vinblastine was reduced to 1.3 ± 0.08-fold ($P < 0.05$). In contrast, the A198C mutation (Fig. 3b) altered the potency of vinblastine to stimulate ATP hydrolysis, with a 5.1-fold reduction in potency to EC_{50} = 13.7 ± 0.3 μM. Consequently, we would define both mutations as affecting the interaction of vinblastine with Pgp.

In the presence of rhodamine 123, the ATPase activity of cysless Pgp was stimulated 2.41 ± 0.23-fold and with a potency of 54 ± 6 μM (Fig. 3c–d, Table 1). The Y953C mutation abrogated the ability of rhodamine to stimulate ATPase activity (Fig. 3c) and this effect is referred to as a "no response" (N.R) in Table 1. Many mutations do not cause any effect on the potency or ability of drugs to stimulate ATP hydrolysis, as shown for the interaction of rhodamine 123 with the A198C P-gp (Fig. 3d).

Fig. 4 provides representative data to illustrate the tryptophan quenching fluorescence assay used to investigate drug binding to Pgp, with the complete analysed data presented in Table 2 (and Figs. S3, S4).

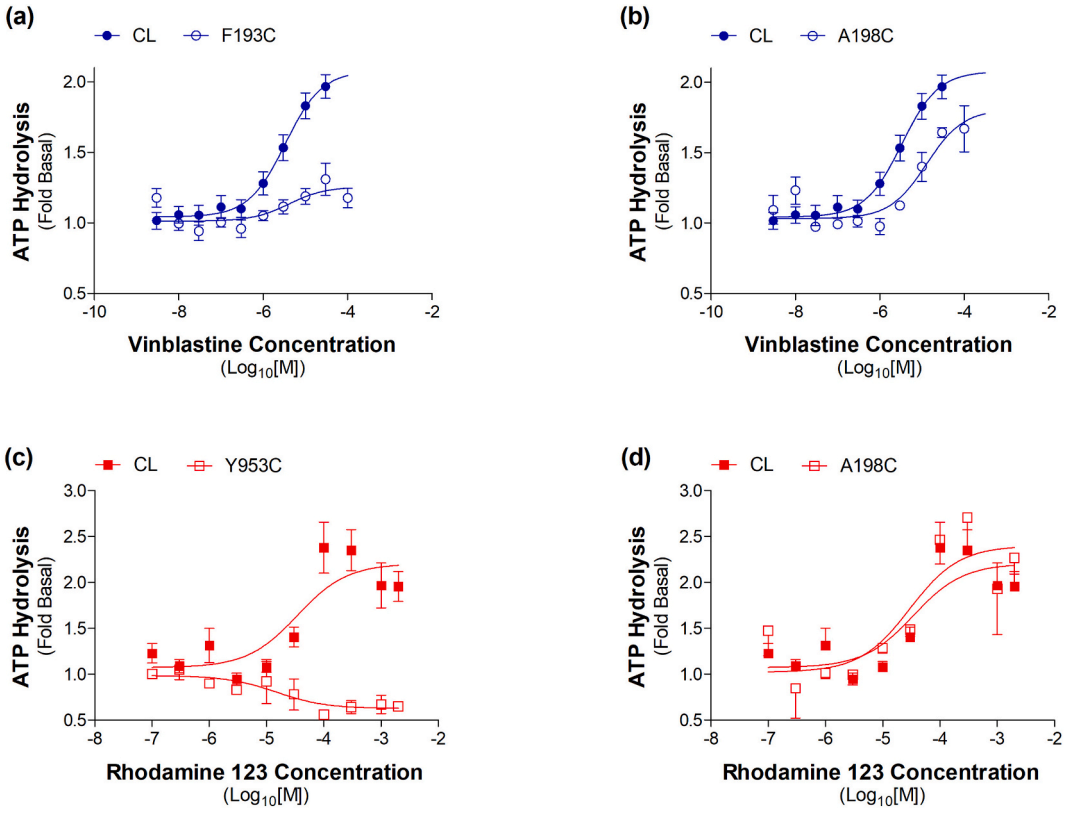

Fig. 3. Drug stimulated ATPase activity of Pgp mutants.
ATPase activity was measured as a function of either vinblastine or rhodamine 123 concentration. Activity of the (a) F193C, (b) A198C, (c) Y953C and (d) A198C mutants was compared to that observed with cysless Pgp. The dose-response relationship was fitted to the data using non-linear regression and the ATPase activity of each mutant in the absence of drug (basal) was assigned a value of 1.0. Data correspond to the mean ± SEM from n = 3–8 independent observations. CL refers to the cysteine-less control protein.

Table 1
The effects of mutations in the putative interface and cavity binding sites on drug stimulated ATPase activity.

	Mutant	Vinblastine		Rhodamine 123		Nicardipine	
		EC_{50} (μM)	Stimulation (fold-basal)	EC_{50} (μM)	Stimulation (fold-basal)	EC_{50} (μM)	Stimulation (fold-basal)
	CL	2.69 ± 0.52	1.94 ± 0.09	54 ± 6	2.41 ± 0.23	0.74 ± 0.11	3.19 ± 0.28
Interfacial site	F193C	0.82 ± 0.46	*1.30 ± 0.08**	*26.4 ± 5.6**	1.96 ± 0.12	1.42 ± 0.46	2.58 ± 0.26
	F194C	2.75 ± 0.67	*1.53 ± 0.13**	40.1 ± 4.9	*1.51 ± 0.15**	0.73 ± 0.10	2.83 ± 0.30
	A198C	*13.7 ± 3.0**	1.80 ± 0.10	41.8 ± 11.7	2.60 ± 0.21	*2.37 ± 0.87**	3.10 ± 0.37
	S344C	7.21 ± 4.28	*1.40 ± 0.08**	35.0 ± 4.9	1.94 ± 0.17	1.04 ± 0.22	2.93 ± 0.15
Cavity site	F72C	2.60 ± 0.70	*1.45 ± 0.12**	*NR**	*NR**	1.38 ± 0.28	3.88 ± 0.44
	Y950C	3.67 ± 0.79	1.61 ± 0.17	*NR**	*NR**	1.02 ± 0.12	4.10 ± 0.82
	Y953C	*NR**	*NR**	*NR**	*NR**	2.32 ± 1.08	3.41 ± 0.09
	I981C	*NR**	*NR**	*NR**	*NR**	1.28 ± 0.28	2.31 ± 0.41

Drug stimulated ATPase activity was measured for each mutant in the presence of varying concentrations of vinblastine, rhodamine 123 or nicardipine. The general dose response relationship was fitted to the data and the potency (EC_{50}) and extent of stimulation (fold basal) were derived. The ATPase activity in the absence of drug was assigned a value of 1.0. All values represent the mean ± SEM from n = 3–8 independent observations and * next to italicised font indicates a statistically significant ($P < 0.05$) difference from cysless (CL) P-gp. NR indicates that the drug did not alter the basal ATPase activity of the mutant.

Panel *(a)* contrasts the binding isotherms derived for vinblastine and rhodamine 123 with cysless P-gp. Vinblastine displayed an apparent binding affinity of K_{APP} = 16.4 ± 1.4 μM and increased the fluorescence intensity by 27.6 ± 2.5 r.f.u, a parameter that resembles the binding capacity (B_{MAX}). Rhodamine 123 displayed an apparent affinity of K_{APP} = 6.6 ± 0.8 μM and a change in fluorescence intensity of 49.3 ± 3.8 r.f.u. Fig. 4b demonstrates the effect of a Y950C mutation on the binding of rhodamine 123. The apparent affinity was unchanged (Table 2); however, the binding capacity was reduced by approximately 25 %.

The following two sections refer to data produced by these assays and the main parameters are provided in Tables 1 and 2. All data sets (with average values) for the two assays with three marker drugs are provided in Supplementary Figs. S1–S4.

3.3. Mutation of the putative interfacial site on drug binding to Pgp

In an earlier investigation we identified that residue M197 in Pgp was involved in the binding of vinblastine [7]. M197 is situated in transmembrane helix 3 (TM3) and according to the *4M1M* structural model, it faces the lipid milieu. Based on the size of vinblastine, it is likely that multiple residues are involved in its binding. Consequently, a further four residues (F193, F194, A198, S344) located proximal to

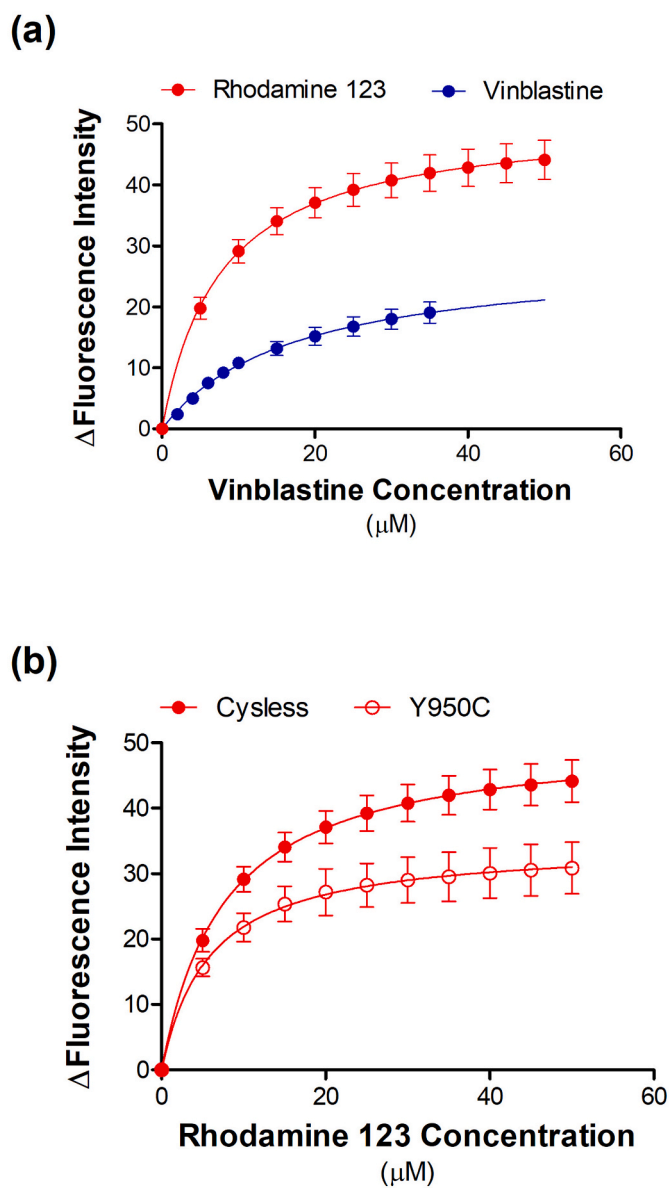

Fig. 4. Drug binding to Pgp – tryptophan quenching analysis.
Quenching of the intrinsic tryptophan fluorescence of Pgp was done in the presence of increasing drug concentration. The change in fluorescence intensity was plotted as a function of drug concentration and the Langmuir Adsorption isotherm was fitted using non-linear regression. (a) Fluorescence quenching was measured in the presence of either vinblastine or rhodamine 123 for cysless Pgp. (b) The extent of fluorescence quenching by rhodamine 123 was measured for the cysless and Y950C mutant of Pgp. All values represent the mean ± SEM from n = 4 independent observations.

M197 were also proposed (according to predictions from the *4M1M* structural model) to contribute to the binding interaction between Pgp and vinblastine. Moreover, the residues are predicted to lie at the protein-lipid interface and three (F193, F194, A198) are located in TM3, which has been proposed to act as a gate to the central cavity. This region encompassing these residues will be referred to as the *interfacial binding site* for the anticancer drug, and Pgp substrate, vinblastine.

In agreement with our predictions, all four residues at the lipid-protein interface affected the interaction of vinblastine with Pgp, Specifically, mutations F193C, F194C and S344C caused significant reductions in the ability of vinblastine to stimulate ATP hydrolysis (Table 1, Fig. S1) and A198C reduced the potency to stimulate. F193C, F194C and A198C mutations caused small alterations in the apparent binding affinity of vinblastine (Table 2) and S344C produced a statistically significant ($P < 0.05$) reduction in K_{APP}.

Based on the structural models we would predict that mutations to the interfacial residues should not perturb the interaction of rhodamine 123 with Pgp. Compared to the widespread effects on vinblastine interaction the prediction is upheld since only the F194C mutation affected the interaction of rhodamine 123, leading to a reduction in the stimulation of ATP hydrolysis (Table 1, Fig. S1).

Similarly, we would predict that mutations at the interfacial site for vinblastine should not markedly affect the interaction of nicardipine with Pgp. This is based on previous data from Mittra et al. [7] that implicated residue T769 (TM8) in the binding of nicardipine to Pgp. Residue T769 is found at an interfacial location on P-gp, although it is located on TM8 and thus distal to the vinblastine interfacial site. This prediction was also supported by the fact that only mutation A198C altered the interaction of nicardipine, by reducing its potency to stimulate ATP hydrolysis (Table 1, Fig. S1).

The functional data reveal that the interfacial site can mediate the interaction of vinblastine with Pgp. Importantly, this site is relatively specific to vinblastine given that mutations within it did not have pronounced, or widespread, effects on the binding of another substrate (rhodamine 123) or an allosteric inhibitor (nicardipine).

3.4. Mutation of the putative cavity site on drug binding to Pgp

Our earlier investigation identified four residues (L65, F336, F978, V982) that contributed to the binding of rhodamine 123 and based on the *4M1M* model, these residues are predicted to reside in the central cavity of Pgp. Using this structural model, a further four residues (F72, Y950, Y953, I981) were selected for analysis to assess their possible contribution to rhodamine 123 binding by Pgp. The region encompassing these residues will be referred to as the *cavity binding site* for the transport substrate rhodamine 123.

The effects of these four mutations on the interaction of rhodamine 123 with Pgp are summarised in Table 2 and Figs. S2 and S4. Specifically, the 2.4-fold stimulation of ATP hydrolysis observed with cysless Pgp, was abrogated by each of the *cavity site* mutations; indicating a major impact on rhodamine 123 interaction. The mutations were associated with minor effects on the quenching of tryptophan fluorescence. Potentially, this suggests that the assay is less susceptible to perturbation by a point mutation; presumably due to the involvement of multiple residues and bonds in the binding of drugs such as vinblastine, rhodamine 123 and nicardipine. The data provide further confirmation of the region in the *central cavity* of Pgp that mediates the interaction of rhodamine 123.

Thus far, the data support our initial hypothesis that interaction with Pgp occurs at the *central cavity* for rhodamine 123 and at the *interfacial site* for vinblastine. However, further analysis of the *cavity site* mutations demonstrated that they also affected the interaction of vinblastine with P-gp (Table 1, Fig. S2). For example, the F72C mutation caused a significant ($P < 0.05$) reduction in the ability of vinblastine to stimulate ATP hydrolysis. Furthermore, vinblastine failed to generate any stimulation of ATP hydrolysis for Pgp containing the Y953C and I981C mutations. In addition, the Y953C and I981C mutations altered the extent to which the endogenous tryptophan fluorescence was quenched. The extent of quenching was increased compared to cysless Pgp, which may be interpreted as an increase in the binding capacity to vinblastine (Table 2, Fig. S4). It is important to note that altered tryptophan fluorescence can occur via direct collisional quenching or long-range effects; consequently, the latter represents an allosteric effect rather than direct binding. Alternatively, there may be a paucity of Trp residues in the region of the mutation, thereby displaying less potential to impact the local environment of a tryptophan. These considerations reflect our use of the term K_{APP} to represent an apparent binding affinity.

Overall, the *cavity site* mutations confirm this region as the location for rhodamine 123 binding and reveal that vinblastine may also interact

Table 2
The effects of mutations in the putative interface and cavity binding sites on apparent drug binding.

	Mutant	Vinblastine		Rhodamine 123		Nicardipine	
		B_{MAX} (ΔRFU)	K_{APP} (μM)	B_{MAX} (ΔRFU)	K_{APP} (μM)	B_{MAX} (ΔRFU)	K_{APP} (μM)
	CL	27.6 ± 2.5	16.4 ± 1.4	49.3 ± 3.8	6.6 ± 0.8	49.7 ± 2.6	4.6 ± 0.6
Interfacial site	F193C	28.1 ± 0.8	21.0 ± 3.1	44.2 ± 2.2	6.7 ± 1.1	41.9 ± 3.0	4.7 ± 0.1
	F194C	26.6 ± 0.9	20.2 ± 1.4	42.4 ± 2.1	8.2 ± 0.5	38.7 ± 1.2	4.4 ± 0.6
	A198C	29.0 ± 1.8	21.9 ± 1.8	50.8 ± 5.6	6.6 ± 0.4	52.9 ± 3.5	5.3 ± 0.2
	S344C	32.0 ± 1.9	*27.0 ± 2.3**	46.5 ± 1.4	8.7 ± 0.8	45.8 ± 2.5	5.0 ± 0.6
Cavity site	F72C	*47.7 ± 6.8**	21.9 ± 1.4	54.0 ± 8.8	6.8 ± 0.8	66.8 ± 1.6	4.8 ± 0.2
	Y950C	43.1 ± 9.9	21.8 ± 0.7	38.7 ± 3.4	5.7 ± 0.6	35.4 ± 5.0	3.9 ± 0.3
	Y953C	*48.5 ± 4.4**	17.3 ± 0.9	54.1 ± 4.0	7.1 ± 0.8	49.6 ± 5.4	4.4 ± 0.2
	I981C	49.3 ± 10.2	14.4 ± 4.1	59.1 ± 3.3	8.4 ± 0.8	57.9 ± 0.5	6.0 ± 0.3

The quenching of intrinsic tryptophan fluorescence was measured for each Pgp mutant in the presence of varying concentrations of vinblastine, rhodamine 123 or nicardipine. The Langmuir Adsorption Isotherm was fitted to the data and the apparent binding affinity (K_{APP}) and maximal change in tryptophan fluorescence (B_{MAX}) were derived. All values represent the mean ± SEM from n = 3–6 independent observations and * next to italicised font indicates a statistically significant ($P < 0.05$) difference from cysless (CL) P-gp.

at the site. It is unlikely to represent a non-specific interaction since none of the mutations affected the interaction of nicardipine with P-gp as assessed by both ATPase activity and quenching of endogenous tryptophan residues.

3.5. Molecular docking analysis of drug binding to Pgp

Molecular docking was undertaken for vinblastine at both the interfacial and cavity sites, in addition to rhodamine 123 at the central aqueous cavity. The use of a human Pgp structure as a template might result in subtle change(s) in the docking of vinblastine or rhodamine 123. Analysis provided nine poses for each drug at the sites. The energetics of binding for the poses were broadly similar (Table S2) and therefore, we decided to classify poses within a "coarse binding site". Residues in proximity to the "coarse binding site" were identified and the distance from that residue to the specific drug were determined. These residues were categorised by the number of poses in which a particular residue is within 5 Å distance to the drug. This scoring system

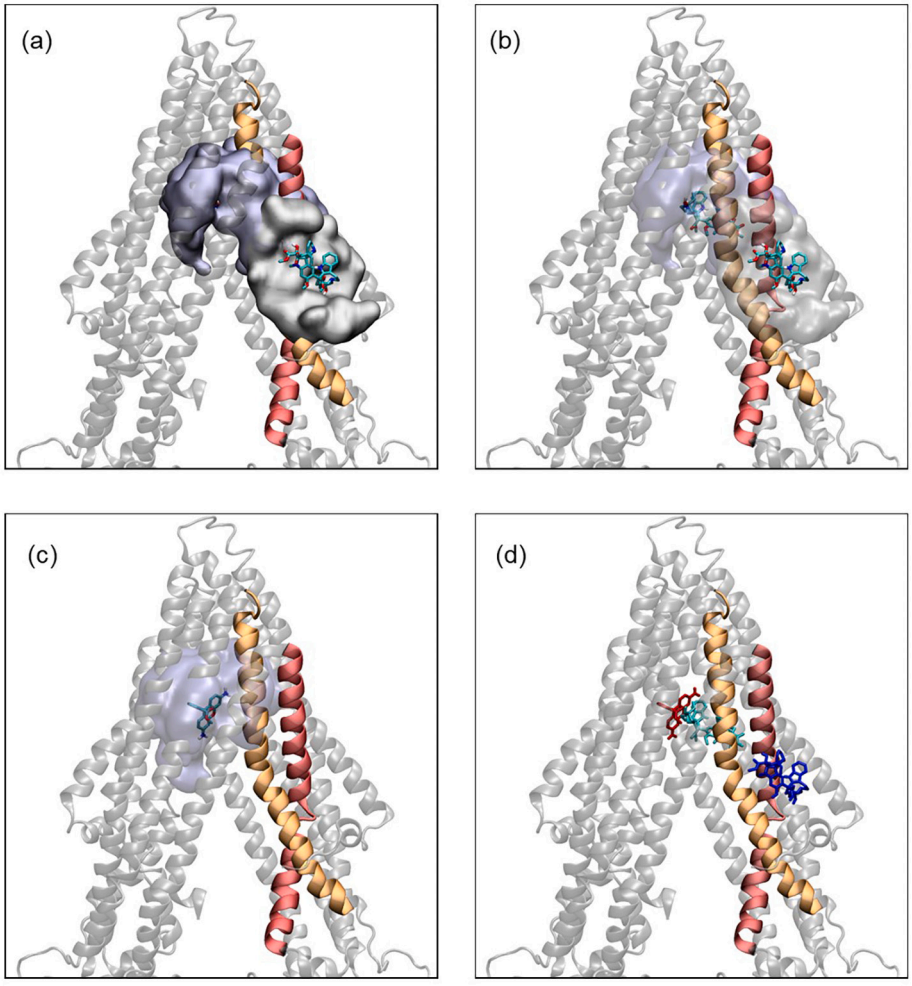

Fig. 5. Docking of vinblastine and rhodamine 123 to the binding sites on Pgp.
Location of the cavity and interfacial binding sites for vinblastine and rhodamine as identified by docking analysis. Pgp is shown as cartoon representation in grey and helices TM3 and TM6 are shown in orange and yellow respectively. The cavity and interfacial binding sites are shown as surface representations in pale blue and grey, respectively. The surface comprises all residues predicted to be involved in binding based on docking analysis. Panel (a) shows vinblastine at the surface site, whilst (b) depicts vinblastine at both the surface and cavity sites. Panel (c) shows rhodamine 123 in the cavity site. Panel (d) depicts vinblastine (blue) at the surface or within the cavity (cyan), in addition to rhodamine 123 in the cavity.

helped generate a heat map to indicate how likely the individual residues are involved in the interaction with vinblastine or rhodamine 123. The scoring and cut-off values are documented in Fig. S5 and Table S2. The representation for vinblastine binding in Fig. S5 demonstrates a considerable contrast between the cavity and interfacial sites. The cavity site contains 49 residues arranged to encase the vinblastine molecule. The interfacial residues of Pgp involved with vinblastine binding did not encase the drug, instead providing a surface for interaction formed by 18 residues.

The binding site residues identified from the docking analysis were used to visualise the surface areas these cavity and interfacial drug binding sites occupy on the protein (Fig. 5). For vinblastine, this representation clearly shows how the interfacial and cavity binding sites are contiguous and TM3/TM6 provide a gate between the two sites (Fig. 5a–b). As indicated above, the site at the protein-lipid interface provides an interaction surface to facilitate vinblastine binding that includes the hydrophobic F193, F194 and A198 residues mutated in the present investigation. The cavity site includes residues F72, Y953 and I981 that were identified in this investigation with an involvement in vinblastine binding. Both experimental and docking data demonstrate a partial overlap of residues between the central cavity localised binding sites for rhodamine123 and vinblastine (Fig. 5d). The cavity binding site for vinblastine also includes several of the residues we have previously identified in the interaction with Pgp – these residues are listed and summarised in Table S1. Moreover, the residues listed in Table S1 are not involved in the interaction with rhodamine 123 and suggest that the central cavity of Pgp has multiple, partly overlapping, drug interaction sites (Fig. 5d).

In general, resolution and organism are only one of many considerations for choosing a structure to undertake docking or modelling analyses. Provided the sequence identity is high between the protein from different organisms and that the structure/mechanisms of transport are similar, the important point is to have a structure of the protein that is in the conformation to which the drug is known to bind to. The latter is the focus of our project. Many of the more recent human structural models obtained using cryo-EM involved Pgp constrained by the incorporation of one (or more) antibody fragments [25,27]. This strategy produced intermediate protein conformations that are difficult to relate to the more established alternating conformations of high and low substrate affinity – a situation we hoped to avoid.

4. Discussion

Identifying the location and chemical properties of substrate binding sites remains at the forefront of efforts to understand the basis of molecular recognition by Pgp. This will finally reveal the pharmacophore and facilitate the development of potent, specific inhibitors. This herculean task remains unresolved despite its origins with early photoaffinity labelling strategies [5,15,42], through to contemporary computational [43–45] and structural approaches [27,46].

Recent progress has been made with allosteric inhibitors [25]; however, investigations in this manuscript have focussed on two transported substrates. The site for rhodamine 123 interaction within the central cavity of Pgp has been further refined with the inclusion of newly identified residues involved in binding. Similarly, several residues within the central cavity, to complement those previously identified, have been found to interact with vinblastine. There is some overlap, but not complete, in the residues that form interaction sites for vinblastine and rhodamine 123. Contributing residues are located on multiple transmembrane helices (TM) that line the cavity, with myriad contributions from TM6 and TM12. Furthermore, additional residues interacting with vinblastine have been observed in a distinct location; namely at the lipid-protein interface, clustered on TM3. This suggests the presence of two distinct binding sites for a single transported substrate, vinblastine. Does Pgp mediate transport using two distinct routes? One via a central conduit is intuitive and supported by a wealth of data [6,9,10,22,25,46,47]. The interfacial site may operate along the outer (or lipid facing) surface of Pgp, but this non-traditional route is potentially akin to the proposed mechanism of a phospholipid flippase. We suggest a more conventional alternative involving a processive transport mechanism for hydrophobic substrates involving *entrapment* from the lipid milieu, *transfer* to the central conduit and subsequent *translocation* across the membrane.

Several lines of data suggested that the initial interaction with numerous Pgp substrates occurs from the non-aqueous environment of biological membranes [14,15]. This led to dubbing Pgp as a "hydrophobic vacuum cleaner" for drugs within the bilayer [15,16]. Selective extraction of hydrophobic substrates, such as vinblastine ($logP = 3.056$), from the vast sea of lipids in biological membranes would be enhanced by a mechanism of *entrapment*. Previous work from our team also identified distinct *entrapment sites* for the hydrophobic compounds nicardipine and paclitaxel; with the amino-acids involved referred to as contact residues [7]. The concept of *entrapment* has precedent within the ABC transporter family. For example, the pyrophosphate moiety of lipid-linked oligosaccharide interacts with a sequence of positively charged residues on the Pglk transporter from *Campylobacter jejuni* [48]. In addition, the phosphorylated isoprenoid moiety of the polysaccharide O-antigen is selectively bound by a gate on the *Wzm/Wzt* transporter at the cytosolic hemileaflet of Gram negative bacteria [49]. In both examples, the *entrapment site* serves a dual purpose; to extract substrates from the lipid milieu and to orientate them for the subsequent translocation event through a central cavity.

This idea is also borne out by the structural data of Nosol et al. [25] suggesting that potent hydrophobic inhibitors of Pgp bind in pairs, with one of the pair found at the lipid-protein interface proximal to TM4 and TM10. The interaction between inhibitors and Pgp is reliant on the presence of hydrophobic residues, with phenylalanine predominant. An analogous strategy can be seen with the multidrug efflux pump AcrB from the resistance nodulation division (RND) protein family – despite the dissimilarity in translocation mechanism [50]. Structural data for AcrB demonstrated the presence of a phenylalanine rich "pit" near the protein surface to ensnare hydrophobic compounds. The *entrapment* site for vinblastine is not simply a non-specific "pit" given that another hydrophobic drug, nicardipine ($logP = 3.535$), did not interact at this site. Furthermore, previous work by our team [19] demonstrated that binding sites for nicardipine and vinblastine share a negative allosteric interaction and that the location of nicardipine (*entrapment*) site is proximal to T769 on TM8 [7].

Ultimately, it appears that drug translocation by Pgp occurs through an alternating access mechanism involving the distinguishing central cavity that was first identified by Rosenberg et al. [12]. The dimensions of this central cavity are considerably greater than most Pgp substrates, which provides multiple individual sites for binding and may even support the simultaneous binding of more than one compound. Site-directed mutagenesis approaches identified a substantial number of amino-acids in Pgp that are likely to contribute to substrate binding [9,10,22,30,51–53] and the advent of structural data for the protein confirmed their location within this central cavity [27,46]. Molecular docking approaches have combined these two streams of research to provide detailed mapping of drug binding in the cavity [43,44,54,55]. The residues we have identified for rhodamine 123 binding agree with these studies and confirm the location of the R-site predicted by in silico approaches. It is clear from the experimental and in silico approaches that defined regions of the cavity interact with specific drugs – i.e. a binding site. However, different binding sites display partial overlap in their constituent amino-acids – as demonstrated here for cavity site residues that interact with both vinblastine and rhodamine 123. It is fair to say that the central cavity has a degree of wiggle room to accommodate the sheer number of possible substrates, which is implicit in conferring poly-specificity.

Our suggestion is that the hydrophobic compound vinblastine is entrapped at the interfacial site (includes residues F193, F194, M197,

A198) and subsequently transferred to a central cavity location that has some overlap (F72, Y950, Y953, I981) with the R-site. In contrast, neither activity assays nor docking approaches were able to demonstrate an interaction site for rhodamine 123 ($logP = 2.256$) at the Pgp-lipid interface. This is in agreement with a transport kinetic investigation [40] demonstrating that rhodamine 123 does not appear to be extracted from the plasma membrane by Pgp and it may directly enter the central cavity.

Previous investigations by our team has identified that the stretch of residues on TM6 (F343 to S349) also plays a crucial role in the interaction with vinblastine [7,56]. How does the transfer from the interfacial to the cavity site occur? Several groups propose the involvement of gates formed by pairs of TM-helices [8,23,25] and we extend this to suggest that residues S344 and F343 constitute the latch. S344 and F343 reside between TM6 and TM3 and mutations markedly affect the interaction between vinblastine and Pgp. Moreover, using fluorescent [53] and paramagnetic probes [57], we have demonstrated that residue 343 in TM6 is highly mobile during transition of Pgp between nucleotide-free, nucleotide-bound and post-hydrolytic conformations. Structural data [25] posits that residue F343 is located in what the authors refer to as the access tunnel that forms in the transition state of Pgp locked by the presence of antibody fragments.

4.1. Conclusion

We have provided evidence that Pgp has an *entrapment site* for vinblastine that facilitates its extraction from the lipid milieu and propose that this may occur for other hydrophobic drugs such as nicardipine. These *entrapment sites* are aligned with gates that enable access of bound substrates (e.g. vinblastine) into the central cavity as Pgp transitions through intermediate conformations. Translocation of substrate across the membrane occurs as this central cavity undergoes a switch from inward to outward facing. Finally, we speculate that inhibitors bound at entrapment sites may perturb conformational transitions and are thus unable to fully enter the central cavity.

Declaration of competing interest

The authors declare that they have no known competing financial interests or personal relationships that could have appeared to influence the work reported in this paper.

Data availability

Data will be made available on request.

Acknowledgements

The authors thank the Australian National University and the Research School of Biology for providing scholarships to S. Iqbal and R. Skrzypek and block grant funding for the project.

Appendix A. Supplementary data

Supplementary data to this article can be found online at https://doi.org/10.1016/j.bbamem.2022.184005.

References

[1] H.L. Pearce, M.A. Winter, W.T. Beck, Structural characteristics of compounds that modulate P-glycoprotein-associated multidrug resistance, Adv. Enzym. Regul. 30 (1990) 357–373.
[2] A. Seelig, A general pattern for substrate recognition by P-glycoprotein, Eur. J. Biochem. 251 (1–2) (1998) 252–261.
[3] S.G. Aller, J. Yu, A. Ward, Y. Weng, S. Chittaboina, R. Zhuo, P.M. Harrell, Y. T. Trinh, Q. Zhang, I.L. Urbatsch, G. Chang, Structure of P-glycoprotein reveals a molecular basis for poly-specific drug binding, Science 323 (5922) (2009) 1718–1722.
[4] S. Dey, M. Ramachandra, I. Pastan, M.M. Gottesman, S.V. Ambudkar, Evidence for two nonidentical drug-interaction sites in the human P- glycoprotein, Proc. Natl. Acad. Sci. U. S. A. 94 (20) (1997) 10594–10599.
[5] L.M. Greenberger, Major photoaffinity drug labeling sites for iodoaryl azidoprazosin in P-glycoprotein are within, or immediately C-terminal to, transmembrane domains 6 and 12, J. Biol. Chem. 268 (15) (1993) 11417–11425.
[6] T.W. Loo, D.M. Clarke, Mapping the binding site of the inhibitor tariquidar that stabilizes the first transmembrane domain of P-glycoprotein, J. Biol. Chem. 290 (49) (2015) 29389–29401.
[7] R. Mittra, M. Pavy, N. Subramanian, A.M. George, M.L. O'Mara, I.D. Kerr, R. Callaghan, Location of contact residues in pharmacologically distinct drug binding sites on P-glycoprotein, Biochem. Pharmacol. 123 (2017) 19–28.
[8] K. Pleban, S. Kopp, E. Csaszar, M. Peer, T. Hrebicek, A. Rizzi, G.F. Ecker, P. Chiba, P-glycoprotein substrate binding domains are located at the transmembrane domain/transmembrane domain interfaces: a combined photoaffinity labeling-protein homology modeling approach, Mol. Pharmacol. 67 (2) (2005) 365–374.
[9] T.W. Loo, D.M. Clarke, Defining the drug-binding site in the human multidrug resistance P-glycoprotein using a methanethiosulfonate analog of verapamil, MTS-verapamil, J. Biol. Chem. 276 (18) (2001) 14972–14979.
[10] T.W. Loo, D.M. Clarke, Determining the dimensions of the drug-binding domain of human P-glycoprotein using thiol cross-linking compounds as molecular rulers, J. Biol. Chem. 276 (40) (2001) 36877–36880.
[11] E.P. Bruggemann, S.J. Currier, M.M. Gottesman, I. Pastan, Characterization of the azidopine and vinblastine binding site of P- glycoprotein, J. Biol. Chem. 267 (29) (1992) 21020–21026.
[12] M.F. Rosenberg, R. Callaghan, R.C. Ford, C.F. Higgins, Structure of the multidrug resistance P-glycoprotein to 2.5 nm resolution determined by electron microscopy and image analysis, J. Biol. Chem. 272 (16) (1997) 10685–10694.
[13] M.F. Rosenberg, R. Callaghan, S. Modok, C.F. Higgins, R.C. Ford, Three-dimensional structure of P-glycoprotein: the transmembrane regions adopt an asymmetric configuration in the nucleotide-bound state, J. Biol. Chem. 280 (4) (2005) 2857–2862.
[14] L. Homolya, Z. Hollo, U.A. Germann, I. Pastan, M.M. Gottesman, B. Sarkadi, Fluorescent cellular indicators are extruded by the multidrug resistance protein, J. Biol. Chem. 268 (29) (1993) 21493–21496.
[15] Y. Raviv, H.B. Pollard, E.P. Bruggemann, I. Pastan, M.M. Gottesman, Photosensitized labeling of a functional multidrug transporter in living drug-resistant tumor cells, J. Biol. Chem. 265 (7) (1990) 3975–3980.
[16] C.F. Higgins, M.M. Gottesman, Is the multidrug transporter a flippase? Trends Biochem. Sci. 17 (1) (1992) 18–21.
[17] D.R. Ferry, M.A. Russell, M.H. Cullen, P-glycoprotein possesses a 1,4-dihydropyridine selective drug acceptor site which is allosterically coupled to a vinca alkaloid selective binding site, Biochem. Biophys. Res. Commun. 188 (1992) 440–445.
[18] C. Martin, G. Berridge, C.F. Higgins, R. Callaghan, The multi-drug resistance reversal agent SR33557 and modulation of vinca alkaloid binding to P-glycoprotein by an allosteric interaction, Br. J. Pharmacol. 122 (4) (1997) 765–771.
[19] C. Martin, G. Berridge, C.F. Higgins, P. Mistry, P. Charlton, R. Callaghan, Communication between multiple drug binding sites on P-glycoprotein, Mol. Pharmacol. 58 (3) (2000) 624–632.
[20] C. Martin, G. Berridge, P. Mistry, C. Higgins, P. Charlton, R. Callaghan, The molecular interaction of the high affinity reversal agent XR9576 with P-glycoprotein, Br. J. Pharmacol. 128 (2) (1999) 403–411.
[21] T.W. Loo, M.C. Bartlett, D.M. Clarke, Identification of residues in the drug translocation pathway of the human multidrug resistance P-glycoprotein by arginine mutagenesis, J. Biol. Chem. 284 (36) (2009) 24074–24087.
[22] T.W. Loo, D.M. Clarke, Location of the rhodamine-binding site in the human multidrug resistance P-glycoprotein, J. Biol. Chem. 277 (46) (2002) 44332–44338.
[23] T.W. Loo, D.M. Clarke, Do drug substrates enter the common drug-binding pocket of P-glycoprotein through "gates"? Biochem. Biophys. Res. Commun. 329 (2) (2005) 419–422.
[24] A.B. Shapiro, V. Ling, Positively cooperative sites for drug transport by P-glycoprotein with distinct drug specificities, Eur. J. Biochem. 250 (1) (1997) 130–137.
[25] K. Nosol, K. Romane, R.N. Irobalieva, A. Alam, J. Kowal, N. Fujita, K.P. Locher, Cryo-EM structures reveal distinct mechanisms of inhibition of the human multidrug transporter ABCB1, Proc. Natl. Acad. Sci. U. S. A. 117 (42) (2020) 26245–26253.
[26] E. Crowley, R. Callaghan, Multidrug efflux pumps: drug binding - gates or cavity? FEBS J. 277 (3) (2010) 530–539.
[27] A. Alam, R. Kung, J. Kowal, R.A. McLeod, N. Tremp, E.V. Broude, I.B. Roninson, H. Stahlberg, K.P. Locher, Structure of a zosuquidar and UIC2-bound human-mouse chimeric ABCB1, Proc. Natl. Acad. Sci. U. S. A. 115 (9) (2018) E1973–E1982.
[28] J. Li, K.F. Jaimes, S.G. Aller, Refined structures of mouse P-glycoprotein, Protein Sci. 23 (1) (2014) 34–46.
[29] A.M. Taylor, J. Storm, L. Soceneantu, K.J. Linton, M. Gabriel, C. Martin, J. Woodhouse, E. Blott, C.F. Higgins, R. Callaghan, Detailed characterization of cysteine-less P-glycoprotein reveals subtle pharmacological differences in function from wild-type protein, Br. J. Pharmacol. 134 (8) (2001) 1609–1618.
[30] J. Storm, M. O'Mara, E. Crowley, J. Peall, P.D. Tieleman, I.D. Kerr, R. Callaghan, Residue G346 in transmembrane segment six is involved in inter-domain communication in P-glycoprotein, Biochemistry 46 (35) (2007) 9899–9910.
[31] E. Crowley, M.L. O'Mara, C. Reynolds, D.P. Tieleman, J. Storm, I.D. Kerr, R. Callaghan, Transmembrane helix 12 modulates progression of the ATP catalytic cycle in ABCB1, Biochemistry 48 (26) (2009) 6249–6258.

[32] D.F. Tang-Wai, S. Kajiji, F. DiCapua, D. de Graaf, I.B. Roninson, P. Gros, Human (MDR1) and mouse (mdr1, mdr3) P-glycoproteins can be distinguished by their respective drug resistance profiles and sensitivity to modulators, Biochemistry 34 (1) (1995) 32–39.
[33] J.C. Taylor, D.R. Ferry, C.F. Higgins, R. Callaghan, The equilibrium and kinetic drug binding properties of the mouse P-gp1a and P-gp1b P-glycoproteins are similar, Br. J. Cancer 81 (5) (1999) 783–789.
[34] K.A. Morrison, A. Akram, A. Mathews, Z.A. Khan, J.H. Patel, C. Zhou, D.J. Hardy, C. Moore-Kelly, R. Patel, V. Odiba, T.J. Knowles, M.U. Javed, N.P. Chmel, T. R. Dafforn, A.J. Rothnie, Membrane protein extraction and purification using styrene-maleic acid (SMA) copolymer: effect of variations in polymer structure, Biochem. J. 473 (23) (2016) 4349–4360.
[35] R. Liu, A. Siemiarczuk, F.J. Sharom, Intrinsic fluorescence of the P-glycoprotein multidrug transporter: sensitivity of tryptophan residues to binding of drugs and nucleotides, Biochemistry 39 (48) (2000) 14927–14938.
[36] S. Gulati, M. Jamshad, T.J. Knowles, K.A. Morrison, R. Downing, N. Cant, R. Collins, J.B. Koenderink, R.C. Ford, M. Overduin, I.D. Kerr, T.R. Dafforn, A. J. Rothnie, Detergent-free purification of ABC (ATP-binding-cassette) transporters, Biochem. J. 461 (2) (2014) 269–278.
[37] S. Chifflet, A. Torriglia, R. Chiesa, S. Tolosa, A method for the determination of inorganic phosphate in the presence of labile organic phosphate and high concentrations of protein: application to lens ATPases, Anal. Biochem. 168 (1) (1988) 1–4.
[38] M.F. Sanner, Python: a programming language for software integration and development, J. Mol. Graph. Model. 17 (1) (1999) 57–61.
[39] W. Humphrey, A. Dalke, K. Schulten, VMD: visual molecular dynamics, J. Mol. Graph. 14 (1) (1996) 27–38, 33–38.
[40] G.A. Altenberg, C.G. Vanoye, J.K. Horton, L. Reuss, Unidirectional fluxes of rhodamine 123 in multidrug-resistant cells: evidence against direct drug extrusion from the plasma membrane, Proc. Natl. Acad. Sci. 91 (11) (1994) 4654.
[41] Q. Qu, J.W. Chu, F.J. Sharom, Transition state P-glycoprotein binds drugs and modulators with unchanged affinity, suggesting a concerted transport mechanism, Biochemistry 42 (5) (2003) 1345–1353.
[42] E.P. Bruggemann, U.A. Germann, M.M. Gottesman, I. Pastan, Two different regions of P-glycoprotein [corrected] are photoaffinity- labeled by azidopine, J. Biol. Chem. 264 (26) (1989) 15483–15488.
[43] E.E. Chufan, K. Kapoor, H.M. Sim, S. Singh, T.T. Talele, S.R. Durell, S.V. Ambudkar, Multiple transport-active binding sites are available for a single substrate on human P-glycoprotein (ABCB1), PLoS One 8 (12) (2013), e82463.
[44] L. Martinez, O. Arnaud, E. Henin, H. Tao, V. Chaptal, R. Doshi, T. Andrieu, S. Dussurgey, M. Tod, A. Di Pietro, Q. Zhang, G. Chang, P. Falson, Understanding polyspecificity within the substrate-binding cavity of the human multidrug resistance P-glycoprotein, FEBS J. 281 (3) (2014) 673–682.
[45] N. Subramanian, K. Condic-Jurkic, A.E. Mark, M.L. O'Mara, Identification of possible binding sites for morphine and nicardipine on the multidrug transporter P-glycoprotein using umbrella sampling techniques, J. Chem. Inf. Model. 55 (6) (2015) 1202–1217.
[46] Y. Kim, J. Chen, Molecular structure of human P-glycoprotein in the ATP-bound, outward-facing conformation, Science 359 (6378) (2018) 915–919, https://doi.org/10.1126/science.aar7389.
[47] J.W. McCormick, P.D. Vogel, J.G. Wise, Multiple drug transport pathways through human P-glycoprotein, Biochemistry 54 (28) (2015) 4374–4390.
[48] C. Perez, A.R. Mehdipour, G. Hummer, K.P. Locher, Structure of outward-facing PglK and molecular dynamics of lipid-linked oligosaccharide recognition and translocation, Structure 27 (4) (2019) 669–678, e665.
[49] Y. Bi, E. Mann, C. Whitfield, J. Zimmer, Architecture of a channel-forming O-antigen polysaccharide ABC transporter, Nature 553 (7688) (2018) 361–365.
[50] R. Nakashima, K. Sakurai, S. Yamasaki, K. Hayashi, C. Nagata, K. Hoshino, Y. Onodera, K. Nishino, A. Yamaguchi, Structural basis for the inhibition of bacterial multidrug exporters, Nature 500 (7460) (2013) 102–106.
[51] E. Crowley, M.L. O'Mara, I.D. Kerr, R. Callaghan, Transmembrane helix 12 plays a pivotal role in coupling energy provision and drug binding in ABCB1, FEBS J. 277 (19) (2010) 3974–3985.
[52] T.W. Loo, D.M. Clarke, Identification of residues in the drug-binding site of human P- glycoprotein using a thiol-reactive substrate, J. Biol. Chem. 272 (51) (1997) 31945–31948.
[53] A. Rothnie, J. Storm, J. Campbell, K.J. Linton, I.D. Kerr, R. Callaghan, The topography of transmembrane segment six is altered during the catalytic cycle of P-glycoprotein, J. Biol. Chem. 279 (33) (2004) 34913–34921.
[54] E.E. Chufan, K. Kapoor, S.V. Ambudkar, Drug-protein hydrogen bonds govern the inhibition of the ATP hydrolysis of the multidrug transporter P-glycoprotein, Biochem. Pharmacol. 101 (2016) 40–53.
[55] L. Wang, L. Zhang, F. Liu, Y. Sun, Molecular energetics of doxorubicin pumping by human P-glycoprotein, J. Chem. Inf. Model. 59 (9) (2019) 3889–3898.
[56] J. Storm, S. Modok, M.L. O'Mara, D.P. Tieleman, I.D. Kerr, R. Callaghan, Cytosolic region of TM6 in P-glycoprotein: topographical analysis and functional perturbation by site directed labeling, Biochemistry 47 (12) (2008) 3615–3624.
[57] J.H. van Wonderen, R.M. McMahon, M.L. O'Mara, C.A. McDevitt, A.J. Thomson, I. D. Kerr, F. Macmillan, R. Callaghan, The central cavity of ABCB1 undergoes alternating access during ATP hydrolysis, FEBS J. 281 (9) (2014) 2190–2201.